Cosubstitution in Ni-Mn-Sb Heusler compounds: Realization of room-temperature reversible magnetocaloric effect driven by second-order magnetic transition

Sheuly Ghosh* and Subhradip Ghosh†
Department of Physics, Indian Institute of Technology Guwahati, Guwahati-781039, Assam, India

(Received 1 October 2019; accepted 3 January 2020; published 3 February 2020)

Materials showing reversible magnetocaloric effect near room temperature are desirable for green refrigeration technology. The compounds in the magnetic Heusler family displaying significant magnetocaloric effect driven by first-order magnetostructural transitions are in vogue. Comparatively, Heusler compounds undergoing second-order magnetic transition near room temperature are less explored in the context of discovering significant magnetocaloric effects, though they can offer certain advantages like less energy cost and hysteresis loss. Using density-functional theory in conjunction with model Hamiltonians, we explore potential room-temperature magnetocaloric materials near second-order magnetic transition by cosubstitution in the Ni-Mn-Sb family. Our investigation on two cosubstituted families, $Ni_{2-x}Fe_xMn_{1+z-y}Cu_ySb_{1-z}$ and $Ni_{2-x}Co_xMn_{1+z-y}Cu_ySb_{1-z}$, discovers significant numbers of compounds with second-order phase transition near room temperature exhibiting significant changes in magnetic entropy, comparable to that observed in the compounds showing inverse magnetocaloric effect near a first-order magnetostructural transition. We provide a systematic way to select potential reversible magnetocaloric compounds and analyze our results from their electronic structures and magnetic exchange interactions.

DOI: 10.1103/PhysRevMaterials.4.025401

I. INTRODUCTION

Materials showing significant magnetocaloric effect (MCE) near room temperature have lately drawn considerable attention due to their applications in environmentally friendly magnetic refrigeration technology. Gd, the prototype magnetocaloric material, shows a high efficiency up to 60% [1], better than conventional refrigerators. The MCE requires large variation in the material's magnetization with temperatures near first- or second-order magnetic phase transitions.

Although, in general, rare-earth-based compounds exhibit large MCE [2–5], Ni-Mn-Z (Z = Ga, Sn, In, Sb) compounds have been found to be quite promising in recent times. The simple structures of Heusler compounds, in conjunction with their cost effectiveness, have been quite useful in expanding the database of multifunctional materials. In most of the Ni-Mn-Z Heuslers, the MCE is observed [6–10] in the vicinity of a first-order magnetostructural transformation. There, the materials undergo a diffusionless structural phase transformation, known as martensitic phase transformation (MPT), from its high temperature cubic austenite phase to a low-temperature, low-symmetry martensitic phase. In general, the MCE, thus obtained due to first-order transition, is higher compared to those obtained in the vicinity of a second-order magnetic transition. However, the materials exhibiting large MCE near a first-order magnetostructural transformation suffer from several disadvantages. The martensitic phase transition costs high energy, which translates into significant hysteresis loss and low efficiency for cooling applications. They also suffer from cracking and fatigue, which severely limit their lifetimes. It is, therefore, of utmost importance, to explore magnetocaloric materials in the Heusler family exhibiting only second-order magnetic phase transitions. They show full reversible effects and have limited mechanical drawbacks. The superior mechanical properties such as ductility, corrosion resistance, and machinability of these materials ease manufacturing and bolster product longevity.

Accordingly, some of the recent studies focused on the exploration of large MCE in magnetic Heusler compounds in the vicinity of a second-order magnetic phase transition. Singh *et al.* [11] experimentally investigated the composition $Ni_2Mn_{1.4}In_{0.6}$ and found a significant negative entropy change (ΔS_{mag}) of 3.3 $J\,kg^{-1}\,K^{-1}$ and 6.3 $J\,kg^{-1}\,K^{-1}$ in an applied field of 2 T and 5 T, respectively, associated with a second-order transition near room temperature (315 K); the ΔS_{mag} being comparable to the benchmark material Gd [2] as a magnetic refrigerant. A reversible magnetic entropy change of 1.02 $J\,kg^{-1}\,K^{-1}$ with moderate refrigeration capacity was obtained across the second-order magnetic transition near room temperature (305 K) in $Mn_{1.58}Fe_{0.34}Ni_{1.64}Sn_{0.44}$ [12] upon a variation of magnetic field by 1.4 T only. A tuneable and fully reversible MCE across the ferromagnetic-paramagetic transition was also realized in $Ni_{1.92}Mn_{1.44}In_{0.64-x}Sn_x$ compounds [13]. The following three major factors behind the large MCE near a second-order phase transition were noted in these experiments: (i) the austenite phase of the system should be stable in the range of operational temperature, (ii) the magnetization should be high, and (iii) second-order magnetic transition temperature, i.e., the Curie temperature (T_c)

*sheuly.ghosh@iitg.ac.in
†subhra@iitg.ac.in

must be close to room temperature for practical refrigeration applications.

Gd, the prototype material for MCE, has a large magnetic moment (≈7.5 μ_B/f.u.) [2] produced by $4f$ electrons. Therefore, for $3d$ transition-metal-based Ni-Mn-Z Heuslers, the target is to achieve a magnetic moment as close to it. Since the largest contribution to the magnetic moment in Ni-Mn-Z compounds comes from the Mn atoms, it is expected that Mn-excess compounds would help increase magnetic moments. The overwhelming majority of Ni-Mn-Z compounds, exhibiting MCE, undergo a first-order magnetostructural transformation. This is typically achieved in Z-deficient, Mn-excess systems. However, contrary to intuition, the magnetic moments of such systems are less than the ones of the stoichiometric compounds Ni_2MnZ because of the antiparallel alignments of Mn spins. One possible way to overcome the dominant antiferromagnetic interaction originating from Mn-Mn interactions in these systems is to substitute Mn or Ni by another transition metal. The substituent, however, should be able to infuse significant ferromagnetic interactions in the system amplifying the net magnetic moment. This has been done in several systems showing first-order magnetostructural transitions, with promising outcomes [14–23]. Investigations showed that there is a delicate balance of relative compositions of the elements that has to be achieved to obtain not only a large magnetic moment but also a desirable martensitic transformation temperature and Curie temperature, simultaneously.

In our recent work on $Ni_2Mn_{1.5}Sb_{0.5}$ compounds [24], we found the proof of this delicate balance upon substitutions of Ni and Mn by Fe, Co, and Cu. The motivation there was to understand the roles of the substituent, the composition, and the substituted elements on magnetic and thermodynamic properties relevant to MCE, and interpret the origin of large MCE in $Ni_2Mn_{1.48+x}Sb_{0.52-x}$ [10], $Ni_{2-x}Co_xMn_{1.56}Sb_{0.44}$ [25], $Ni_{2-x}Co_xMn_{1.52}Sb_{0.48}$ [26,27], and $Ni_2Mn_{1.52-x}Fe_xSb_{0.48}$ [28]. We found that (i) substitution of Mn with Cu brings the magnetization up, and the T_c down, close to room temperature, and (ii) substitution of Ni with Fe(Co) bolsters the magnetization, reduces (increases only slightly) T_c and provides more stability to the austenite phase. This indicates that to explore off-stoichiometric Ni-Mn-Sb to our advantage, in the context of large room-temperature MCE near a second-order phase transition, substitutions of at least two elements simultaneously (cosubstitution) can be useful. This strategy has been adopted earlier successfully [29–31] for materials undergoing first-order magnetostructural transitions.

In what follows, in the present work, we have explored possible members in the cosubstituted $Ni_2Mn_{1+z}Sb_{1-z}$ family which are promising in exhibiting MCE near room temperature by adopting a strategy of substituting specific elements at select sites. The search for compounds with target properties was narrowed down further by imposing certain criteria based upon available information. We have found a good number of materials with significant changes in entropy, due to the second-order magnetic phase transition, that can be useful for cooling applications. The greater significance of this work is that it opens up possibilities to discover more such materials in the Heusler family by adopting the same strategy.

II. COMPUTATIONAL METHODS

In the present work, electronic structure calculations are done with spin-polarized density-functional-theory (DFT)-based projector augmented wave (PAW) method as implemented in VIENNA *Ab initio* SIMULATION PACKAGE (VASP) [32–34]. The valence electronic configurations used for the Mn, Fe, Co, Ni, Cu, and Sb PAW pseudopotentials are $3d^6 4s$, $3d^7 4s$, $3d^8 4s$, $3d^8 4s^2$, $3d^{10} 4s$, and $5s^2 5p^3$, respectively. For all calculations, we use the Perdew-Burke-Ernzerhof implementation of generalized gradient approximation for exchange-correlation functional [35]. An energy cutoff of 550 eV, and a Monkhorst-Pack $11 \times 11 \times 11$ k mesh was used for self-consistent calculations. A larger k mesh of $15 \times 15 \times 15$ is used for the density of states calculations of all the structures. The convergence criteria for the total energies and the forces on individual atoms are set to 10^{-6} eV and 10^{-2} eV/Å, respectively.

The stabilities of the compounds against decomposition into its components are checked by computing the formation energies, defined by

$$E_f = E_{\text{tot}} - \sum_i n_i E_i. \tag{1}$$

E_{tot} is the total energy of the systems, i represents the atoms in the unit cell, and n_i is the concentration of the ith atom. E_i is the total energy of the element i in its bulk ground state.

To compute the Curie temperature T_c of a compound, we first calculate the magnetic pair exchange parameters using multiple scattering Green's function formalism (KKR) as implemented in SPRKKR code [36]. Here, the spin part of the Hamiltonian is mapped to a Heisenberg model:

$$H = -\sum_{\mu,\nu} \sum_{i,j} J_{ij}^{\mu\nu} \mathbf{e}_i^{\mu} . \mathbf{e}_j^{\nu}. \tag{2}$$

μ, ν represent different sublattices, i, j represent atomic positions and $\mathbf{e}_i^{\mu}$ denotes the unit vector along the direction of magnetic moments at site i belonging to sublattice μ. The $J_{ij}^{\mu\nu}$s are calculated from the energy differences due to infinitesimally small orientations of a pair of spins within the formulation of Liechtenstein *et al.* [37]. To calculate the energy differences by the SPRKKR code, a full-potential spin-polarized scalar relativistic Hamiltonian with angular momentum cutoff $l_{\max} = 3$ is used along with a converged k mesh for Brillouin zone integrations. The Green's functions are calculated for 32 complex energy points distributed on a semicircular contour. The energy convergence criterion is set to 10^{-5} eV for the self-consistent cycles. These exchange parameters are then used for the calculation of T_c. The Curie temperatures are estimated with two different approaches: the mean-field approximation (MFA) [38,39] and the Monte Carlo simulation (MCS) method [40–42]. Details of the calculations using these methods are given in Ref. [43].

For an estimation of the changes in magnetic entropy (ΔS_{mag}) due to the application of a magnetic field, we use the Potts model [44,45] instead of Heisenberg model. The Hamiltonian is given by Eq. (3):

$$H = -\sum_{\langle i,\, j \rangle}^{NN} J_{ij}(2\delta_{S_i,\, S_j} - 1) - g\mu_B \mu_0 H_{\text{ext}} \sum_i^N \delta_{S_i,\, S_g}. \tag{3}$$

Here, the first term represents the magnetic interactions at different lattice sites; $J_{i,j}$ being the exchange parameters involving sites i and j, S_i the spin defined on the lattice site i=1, 2,....., N and N the total number of atoms considered in the simulation cell. The second term represents the coupling of the spin system to the external magnetic field H_{ext} along the direction of ghost spin variable S_g. μ_B is the Bohr magneton, g is the Lande factor (here $g = 2$).

At a given temperature, the system is first equilibrated using MCS method. The magnetic specific heat (C_{mag}) and the magnetic entropy (S_{mag}) in an external field are then calculated using Eqs. (4) and (5), respectively. Finally, the magnetocaloric parameter, i.e., the isothermal change in magnetic entropy due to the application of an external field, is calculated by Eq. (6):

$$C_{\text{mag}}(T, H_{\text{ext}}) = \frac{1}{N}\sum_{i}^{N}\frac{\langle H^2\rangle - \langle H\rangle^2}{k_B T^2}, \tag{4}$$

$$S_{\text{mag}}(T, H_{\text{ext}}) = \frac{1}{N}\int_0^T dT\frac{C_{\text{mag}}(T, H_{\text{ext}})}{T}, \tag{5}$$

$$\Delta S_{\text{mag}}(T, H_{\text{ext}}) = S_{\text{mag}}(T, H_{\text{ext}}) - S_{\text{mag}}(T, 0). \tag{6}$$

The MCS using the classical Heisenberg Hamiltonian treats the spins as classical variables which may take on continuous values and hence do not reproduce the saturation value of the magnetic entropy [46]. Thus, to calculate the saturation value of the magnetic entropy, we have used the q-state Potts model, in which the spin variables can take discrete values.

III. RESULTS AND DISCUSSIONS

Taking a cue from our recent findings [24] and available experimental results [10,25–28], as discussed in Sec. I, we choose two cosubstituted Mn-excess, Sb-deficient Ni-Mn-Sb families: (i) $Ni_{2-x}Fe_xMn_{1+z-y}Cu_ySb_{1-z}$ (denoted as Fe@Ni-Cu@Mn) and (ii) $Ni_{2-x}Co_xMn_{1+z-y}Cu_ySb_{1-z}$ (denoted as Co@Ni-Cu@Mn). It is to be noted that the concentration of Sb is also a variable, as the content of Sb is a critical parameter in the stabilization of the austenite phase [47]. The austenite ($L2_1$ Heusler) phase of the systems (space group 225) is modeled by a 16-atom conventional cubic cell with the number of positions for Ni, Mn, and Sb being 8, 4, and 4 respectively. The cosubstituted systems are generated by replacing the atoms by the substituents in a systematic way. As a consequence of the size of the cell, compositions with arbitrary x, y, or z cannot be modeled. In our work, x and z vary independently, the ranges being 0 to 1.5 and 0.25 to 0.75, respectively. The variable y is constrained to be less than or equal to the value of z. Each variable can be changed by an amount of 0.25 only, due to the finite size of the cell.

Previous experimental and theoretical investigations have confirmed that the entropy change evolves as a consequence of the variations in the degree of $L2_1$ atomic order, i.e., the site occupancy of different atoms in a given composition, brought by thermal treatments. Ghosh and Mandal [48] observed a decrease in T_M and an increase in T_c for $Ni_2Mn_{1.46}Sn_{0.54}$ Heusler alloys upon annealing at different time intervals. Sánchez-Alarcos *et al.* [49] showed that quenching temperature and the subsequent heat treatment change the site occupancy of the alloy, affecting the martensitic transformation temperature (T_M) in Ni_2MnGa-based alloys. Theoretical investigations [42,50,51] also showed that the substituent $3d$-transition metal does not always prefer to occupy the site of substitution. Our recent study on substituted $Ni_2Mn_{1.5}Sb_{0.5}$ compounds corroborates this [24]. Therefore, we first optimize the site occupancy and magnetic structures for each of the systems considered, by minimizing the total energy for each composition. We find that the optimized configurations exactly mimic the ones found in the previous two works on Mn-excess, Sb-deficient Ni_2MnSb [47], and single substituted (by Fe, Co, or Cu) $Ni_2Mn_{1.5}Sb_{0.5}$ [24].

After obtaining the ground-state atomic order (site occupancy pattern) and magnetic configurations, we calculate the magnetic moments and Curie temperatures T_c in their austenite phases. The T_c is calculated by the MFA method. The calculations are done by first fixing z that is the excess concentration of Mn with respect to the stoichiometric composition Ni_2MnSb, and then varying x and y independently. The results are shown in Fig. 1.

A. Selection of compounds with potential to exhibit large MCE

To get a significant MCE near room temperature, arising out of a second-order magnetic transition, a large magnetic moment in the austenite phase and a T_c close to room temperature are the requirements. The other requirement is that the austenite phase is stable down to low temperatures or, in other words, no MPT occurs, from the point of view of DFT results at $T = 0$ K. Accordingly, we adopt the following strategy to choose the compounds for final investigations:

(i) From the results on magnetic moments and T_c^{MFA}, as shown in Fig. 1, we select only those compositions (the ranges of x, y, z) whose magnetic moment M_A in the austenite phase satisfies the criterion $M_A \geqslant 4.5\ \mu_B$/f.u., and the magnetic transition temperature (T_c^{MFA}) in the austenite phase satisfies $200\,\text{K} \leqslant T_c^{\text{MFA}} \leqslant 450$ K condition. The condition on M_A is in accordance with the existing results on Heusler compounds showing reasonable MCE. A vast range of T_c^{MFA}, around the room temperature value of 300 K, is considered since MFA is known to overestimate or underestimate the transition temperature quite often.

(ii) Once the compounds satisfying conditions in (i) are selected, their formation energies are calculated to check the stabilities against decomposition into its components. The compounds having negative formation energies are selected for further inspection. Their total energy profiles as a function of tetragonal distortions are examined to check whether a tetragonal phase is energetically favorable. The ones with their austenite phases having the lowest total energies are finally selected for computations of the quantities related to MCE.

Summarizing the results in Fig. 1, we list, in Table I, the ranges of x, y, z over which the compounds satisfy the conditions given in (i). We find that, in comparison to Co-Cu cosubstituted compounds (Co@Ni-Cu@Mn), there are more number of Fe-Cu co-substituted compounds (Fe@Ni-Cu@Mn) that satisfy the condition (i). For the former family, the comparatively less number is mostly due to very high

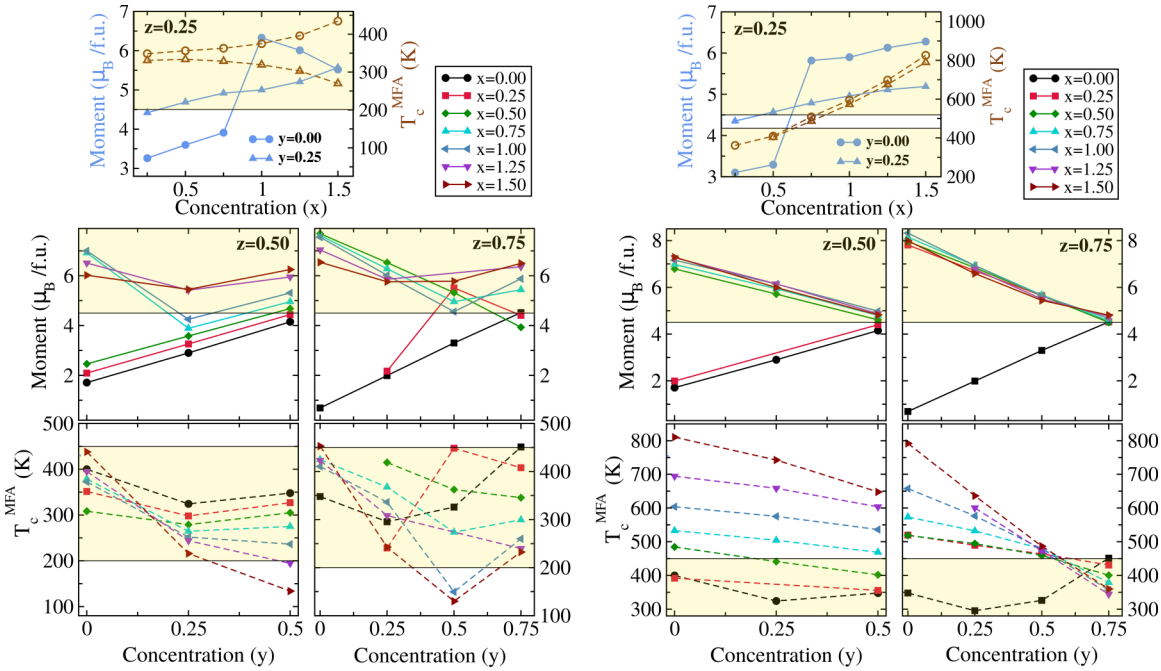

FIG. 1. Variations in the calculated magnetic moments (M_A) and mean-field-approximated Curie temperatures (T_c^{MFA}) with concentrations (x, y, and z) in the austenite phases of (left) $Ni_{2-x}Fe_xMn_{1+z-y}Cu_ySb_{1-z}$(Fe@Ni-Cu@Mn) and (right) $Ni_{2-x}Co_xMn_{1+z-y}Cu_ySb_{1-z}$(Co@Ni-Cu@Mn) systems. Shaded regions mark the composition ranges that satisfy $M_A \geqslant 4.5\ \mu_B$/f.u. and $200\,K \leqslant T_c^{MFA} \leqslant 450\,K$.

values of T_c^{MFA}. In both families, most of the compounds which fail to satisfy the condition on M_A have the Mn spins antialigned, reducing the magnetic moments. The results on formation energies of the compounds selected based upon the condition (i) are shown in Table II. For calculations of formation energies, we have considered bcc-Mn, bcc-Fe, hcp-Co, fcc-Ni, fcc-Cu, and trigonal-Sb as ground-state structures in their elemental phases. The formation energies show the following trend: (a) excess in Mn and deficiency in Sb decreases the stability of the system; (b) for a fixed Sb concentration, Cu substitution at the expense of Mn decreases the stability and for fixed concentration of substituted Mn and Cu, Fe/Co substitution at the expense of Ni further decreases the stability of the system; and (c) Co substitution at the expense of Ni is more favorable than Fe substituting Ni. These observations are in agreement with previous theoretical studies on Ni-Mn-based Heusler compounds [42,51]. In summary, all compounds in the family of Co@Ni-Cu@Mn can form from the point of enthalpy, while the amount of Fe is critical in formation of compounds in the family of Fe@Ni-Cu@Mn.

Next, we check whether the compounds with negative formation energy undergo structural phase transformations under a tetragonal deformation. To this end, we distort the austenite $L2_1$ structure along the z axis by keeping the volume at the equilibrium value of the austenite phase and compute the total energy of the system as a function of the tetragonal distortion given by (c/a). Typical profiles of compounds with stable austenite phases down to low temperatures exhibit the total energy minimum at $(c/a) = 1$ while those undergoing MPT will have their minima at $(c/a) \neq 1$. Some of these profiles computed in the present study are shown and explained in detail in Sec. III, Ref. [43]. In Table II, we list the structurally stable phase of each compound: there N means a tetragonal phase has the lowest energy implying an MPT will take

TABLE I. The compositions of $Ni_{2-x}Fe_xMn_{1+z-y}Cu_ySb_{1-z}$ and $Ni_{2-x}Co_xMn_{1+z-y}Cu_ySb_{1-z}$ which satisfy the criterion of $M_A \geqslant 4.5\ \mu_B$/f.u. and $200\,K \leqslant T_c^{MFA} \leqslant 450\,K$, as seen from results in Fig. 1, are summarized.

$Ni_{2-x}Fe_xMn_{1+z-y}Cu_ySb_{1-z}$			$Ni_{2-x}Co_xMn_{1+z-y}Cu_ySb_{1-z}$	
$z = 0.25$	$z = 0.50$	$z = 0.75$	$z = 0.50$	$z = 0.75$
$x = 1.00, y = 0.00$	$x = 0.50, y = 0.46$–0.50	$x = 0.25, y = 0.43$–0.75	$x = 0.50, y = 0.20$–0.50	$x = 0.25, y = 0.56$–0.75
$x = 1.25, y = 0.00$	$x = 0.75, y = 0.00$–0.20 & 0.40–0.50	$x = 0.50, y = 0.25$–0.65		$x = 0.50, y = 0.56$–0.75
$x = 1.50, y = 0.00$	$x = 1.00, y = 0.00$–0.23 & 0.30–0.50	$x = 0.75, y = 0.00$–0.75		$x = 0.75, y = 0.56$–0.75
$x = 0.50, y = 0.25$	$x = 1.25, y = 0.00$–0.50	$x = 1.00, y = 0.00$–0.43 & 0.62–0.75		$x = 1.00, y = 0.56$–0.75
$x = 0.75, y = 0.25$	$x = 1.50, y = 0.00$–0.30	$x = 1.25, y = 0.00$–0.75		$x = 1.25, y = 0.56$–0.75
$x = 1.00, y = 0.25$		$x = 1.50, y = 0.00$–0.34 & 0.67–0.75		$x = 1.50, y = 0.56$–0.75
$x = 1.25, y = 0.25$				
$x = 1.50, y = 0.25$				

TABLE II. Lattice parameter (a_0), magnetic moment (M_A), mean-field-approximated Curie temperature (T_c^{MFA}), formation energies (E_f) for select compositions (Table I) among $Ni_{2-x}Fe_xMn_{1+z-y}Cu_ySb_{1-z}$(Fe@Ni-Cu@Mn) and $Ni_{2-x}Co_xMn_{1+z-y}Cu_ySb_{1-z}$ (Co@Ni-Cu@Mn) compounds in their austenite phases. The result on the stability of the austenite phase is also tabulated: Y stands for the stability of the austenite phase down to low temperatures. Boldfaces indicate the compositions which satisfy the criteria of negative formation energy and stable austenite phase along with conditions on M_A and T_c^{MFA}. The Monte Carlo simulated Curie temperature (T_c^{MCS}) and maximum change in isothermal magnetic entropy (ΔS_{mag}) values around their corresponding T_c^{MCS} in an external field of 2 T are shown for these compositions only.

Compound & composition	a_0 (Å)	M_A (μ_B/f.u.)	T_c^{MFA} (K)	E_f (eV/f.u.)	Stability of austenite	T_c^{MCS} (K)	$-\Delta S_{mag}$ (J kg^{-1} K^{-1})
$Ni_{2-x}Fe_xMn_{1+z-y}Cu_ySb_{1-z}$							
$z = 0.25$							
$x = 1.00$, $y = 0.00$	5.98	6.35	375.0	−0.181	Y	414	4.55
$x = 1.25$, $y = 0.00$	5.95	6.00	395.9	−0.116	Y	430	7.08
$x = 1.50$, $y = 0.00$	5.92	5.50	434.5	−0.029	Y	450	6.52
$x = 0.50$, $y = 0.25$	5.97	4.69	333.5	−0.348	Y	350	4.03
$x = 0.75$, $y = 0.25$	5.96	4.92	328.8	−0.222	Y	348	3.97
$x = 1.00$, $y = 0.25$	5.95	5.00	319.3	−0.082	Y	341	5.39
$x = 1.25$, $y = 0.25$	5.94	5.21	302.8	0.051			
$x = 1.50$, $y = 0.25$	5.94	5.57	270.0	0.173			
$z = 0.50$							
$x = 0.50$, $y = 0.50$	5.89	4.65	304.9	−0.174	Y	286	4.49
$x = 0.75$, $y = 0.00$	5.92	6.89	378.6	−0.219	Y	400	4.19
$x = 0.75$, $y = 0.50$	5.89	4.94	275.0	−0.022	Y	260	3.29
$x = 1.00$, $y = 0.00$	5.91	7.00	372.5	−0.115	Y	419	3.88
$x = 1.00$, $y = 0.50$	5.88	5.31	236.4	0.143			
$x = 1.25$, $y = 0.00$	5.88	6.50	395.1	−0.031	Y	449	4.32
$x = 1.25$, $y = 0.25$	5.86	5.40	243.8	0.124			
$x = 1.25$, $y = 0.50$	5.90	5.93	194.5	0.261			
$x = 1.50$, $y = 0.00$	5.85	6.01	438.0	0.050			
$x = 1.50$, $y = 0.25$	5.84	5.40	215.8	0.214			
$x = 1.75$, $y = 0.00$	5.82	5.53	460.6	0.120			
$x = 1.75$, $y = 0.25$	5.84	5.65	163.0	0.306			
$x = 2.00$, $y = 0.00$	5.80	5.10	457.4	0.198			
$x = 2.00$, $y = 0.25$	5.84	5.87	155.5	0.397			
$z = 0.75$							
$x = 0.25$, $y = 0.50$	5.83	5.53	448.4	−0.240	N		
$x = 0.25$, $y = 0.75$	5.81	4.43	407.9	−0.167	N		
$x = 0.50$, $y = 0.25$	5.84	6.54	418.8	−0.174	N		
$x = 0.50$, $y = 0.50$	5.81	5.33	362.4	−0.078	N		
$x = 0.75$, $y = 0.25$	5.82	6.27	367.7	−0.045	N		
$x = 0.75$, $y = 0.50$	5.79	4.95	273.8	0.079			
$x = 0.75$, $y = 0.75$	5.82	5.38	299.5	0.179			
$x = 1.00$, $y = 0.00$	5.83	7.51	410.5	−0.052	N		
$x = 1.00$, $y = 0.25$	5.79	6.02	336.3	0.076			
$x = 1.00$, $y = 0.75$	5.82	5.84	260.0	0.336			
$x = 1.25$, $y = 0.00$	5.80	7.02	423.1	0.033			
$x = 1.25$, $y = 0.25$	5.78	5.90	308.3	0.185			
$x = 1.25$, $y = 0.75$	5.84	6.30	239.8	0.460			
$x = 1.50$, $y = 0.00$	5.77	6.53	452.8	0.100			
$x = 1.50$, $y = 0.25$	5.76	5.73	242.6	0.255			
$x = 1.50$, $y = 0.75$	5.83	6.44	232.4	0.603			
$Ni_{2-x}Co_xMn_{1+z-y}Cu_ySb_{1-z}$							
$z = 0.50$							
$x = 0.50$, $y = 0.25$	5.92	5.73	441.1	−0.752	N		
$x = 0.50$, $y = 0.50$	5.89	4.64	401.9	−0.696	Y	484	1.51

TABLE II. *(Continued.)*

Compound & composition	a_0 (Å)	M_A (μ_B/f.u.)	T_c^{MFA} (K)	E_f (eV/f.u.)	Stability of austenite	T_c^{MCS} (K)	$-\Delta S_{mag}$ (J kg^{-1} K^{-1})
$z = 0.75$							
$x = 0.25, y = 0.50$	5.84	5.62	464.1	−0.525	N		
$x = 0.25, y = 0.75$	5.81	4.53	430.9	−0.468	Y	420	1.90
$x = 0.50, y = 0.50$	5.83	5.66	459.5	−0.658	Y	503	2.40
$x = 0.50, y = 0.75$	5.80	4.53	400.5	−0.571	Y	442	1.71
$x = 0.75, y = 0.50$	5.82	5.71	479.0	−0.781	Y	552	2.79
$x = 0.75, y = 0.75$	5.79	4.52	378.9	−0.659	Y	440	2.00
$x = 1.00, y = 0.50$	5.80	5.62	479.0	−0.893	Y	560	3.62
$x = 1.00, y = 0.75$	5.78	4.68	356.7	−0.745	Y	389	1.33
$x = 1.25, y = 0.50$	5.78	5.44	473.4	−1.00	Y	535	4.26
$x = 1.25, y = 0.75$	5.78	4.75	344.2	−0.833	Y	330	2.49
$x = 1.50, y = 0.50$	5.77	5.34	486.6	−1.115	Y	494	4.74
$x = 1.50, y = 0.75$	5.77	4.81	360.0	−0.921	Y	370	3.19

place, and thus the austenite phase is not stable, while Y denotes a stable austenite phase. Finally, we select only those compounds (the compositions of these compounds are the ones boldfaced in Table II) which have negative formation energy and stable austenite phase [condition (ii) above] for computations of their T_c (by the more accurate MCS method) and the isothermal entropy change (ΔS_{mag}).

B. Quantification of parameters important for MCE: Calculations of Curie temperature by MCS method (T_c^{MCS}) and changes in magnetic entropy (ΔS_{mag})

Quantification of relevant physical quantities is important to assess the potentials of the compounds selected for magnetocaloric applications driven by a second-order magnetic transition. Having ascertained a stable cubic phase, a negative enthalpy of formation, and a substantial magnetic moment, we now compute the two most important quantities: the Curie temperature T_c and the maximum change in isothermal magnetic entropy (ΔS_{mag}). Although the T_c was already calculated once to select potential compounds, here we employ the more accurate MCS method for the purpose of quantification as accurate as possible. The results obtained by MCS on a Heisenberg model, denoted as T_c^{MCS}, are shown in Table II. We find that, in general, T_c^{MCS} are higher than T_c^{MFA}. However, in about 50% cases, the disagreement is within 10–20 K. It is to be noted that, in general, it is the T_c^{MFA} that overestimates the experimental Curie temperature while T_C^{MCS} is closer to it. However, in the case of Heusler compounds, there are cases [45,52] where T_c^{MFA} are underestimated with respect to either the experimental results or T_c^{MCS}. In the absence of experimental results in the present case, it is thus difficult to predict which approximation performs better.

Experimental results on the compounds considered in this work are yet to be available. Thus, for the quantitative estimations of ΔS_{mag} to be reliable and convincing, we first benchmark our calculations against a similar system where experimental results are available. We, therefore, compute maximum ΔS_{mag} around corresponding T_c^{MCS} for $Ni_2Mn_{1.4}In_{0.6}$, the compound that showed significant MCE at second-order magnetic transition near room temperature [11]. The details of the calculation are discussed in Ref. [43] (Sec. II). Our obtained ΔS_{mag} of -4.3 J kg^{-1}K^{-1} and -5.81 J kg^{-1}K^{-1} in an applied field of 2 T and 5 T, respectively, around $T_c = 388$ K, agree well with the experimental values (-3.3 J kg^{-1}K^{-1} and -6.3 J kg^{-1}K^{-1} in 2 T and 5 T, respectively). Our calculated T_c is higher than the experimental value by about 70 K. Nevertheless, since the discrepancies between theory and experimental values are not significant, we employ the procedure to compute ΔS_{mag} as a function of temperature in a magnetic field change of 2 T for all the select compounds (boldfaced in Table II) and some of them are shown in Fig. 2, Ref. [43]. The obtained maximum ΔS_{mag} values around their corresponding T_c^{MCS} values for all the compositions (Table II) are found to be comparable to those of the prototype material Gd [2] as well as various Heusler compounds undergoing first-order magnetostructural transitions. For example, ΔS_{mag} of 7.08 J kg^{-1}K^{-1} obtained for $Ni_{0.75}Fe_{1.25}Mn_{1.25}Sb_{0.75}$ is comparable to 7.3 J kg^{-1}K^{-1} and 7.9 J kg^{-1}K^{-1} observed experimentally for $Ni_{1.72}Co_{0.28}Mn_{1.56}Sb_{0.44}$ and $Ni_{1.68}Co_{0.32}Mn_{1.56}Sb_{0.44}$, respectively, in a field of 1 T [25]. From our calculations, we find that though Co-Cu cosubstituted series has more compounds showing non-negligible MCE near room temperature, the entropy changes in Fe-Cu cosubstituted compounds are much higher. We also find that regardless of the series, both T_c and ΔS_{mag} decrease upon addition of Cu, when concentrations of other constituents are kept fixed.

Having observed significant MCE near second-order magnetic phase transition for a number of compounds obtained by cosubstitution in Ni-Mn-Sb, we now try to understand (i) the structural phase stability, (ii) the nature of variations in the magnetic moments with changes in composition, and (iii) variations in the T_c, as obtained from our calculations. These three were the important aspects of selecting compounds, potential for magnetocaloric applications; hence, a microscopic understanding is desirable.

1. Analysis of structural phase stability from electronic structures

In this subsection, we analyze the density of states to understand the stabilization of the austenite phases in the compounds with changes in the compositions of the

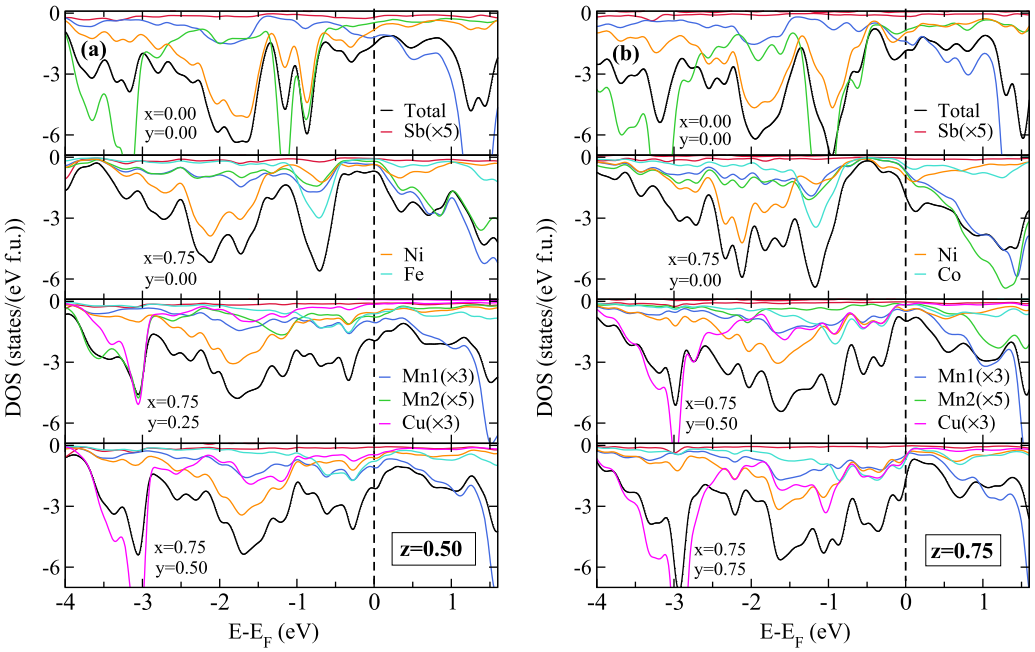

FIG. 2. The minority band total and partial density of states (DOS) for (a) $Ni_{2-x}Fe_xMn_{1+z-y}Cu_ySb_{1-z}$ and (b) $Ni_{2-x}Co_xMn_{1+z-y}Cu_ySb_{1-z}$ systems in their austenite phases. The zero energy is set at Fermi energy (E_F). Mn1 and Mn2 denote Mn atoms at its own site and at other sites in $L2_1$ structure, respectively.

co-substituents. For this, we show the total and atomic densities of states of compounds with z, x fixed at 0.5 and 0.75, respectively, and y varying from 0–0.5 in Fe@Ni-Cu@Mn family. The same is shown for compounds with z, x both fixed at 0.75 with y varying from 0–0.75 in Co@Ni-Cu@Mn family. To ascertain that the austenite phases are stable, the total energy profiles of these compounds have been shown in Fig. 3, Ref. [43]. The total and atomic density of states are also shown in Fig. 4, Ref. [43]. Here we only analyze the minority density of states because, in Ni-Mn-Sb compounds, the structural phase stability can be explained by features in the density of states of the minority bands near Fermi level.

In Ni-Mn-Sb systems, a competition between the strength of the Jahn-Teller instability and the strength of the covalent bonding due to Ni-d and Sb-p minority states drives the phase stability [47]. In stoichiometric Ni_2MnSb, the stability of the austenite phase is driven by the pseudogap at around 1 eV below the Fermi level, generated by Ni-Sb covalent bonding. When Mn is substituted at the expense of Sb ($z \neq 0$, $x = 0$, $y = 0$), the pseudogap is filled by states of Mn atoms at Sb site (i.e., Mn2 atoms), whose spins are antiparallel to those of Mn1 atoms (the ones at original site of Mn). This results in weakening of the covalent bonding. Consequently, Jahn-Teller instability, manifested by the presence of substantial states at the Fermi level, increases, resulting in a MPT, as discussed in Ref. [47]. It is to be noted that in Ni-Mn-based compounds undergoing Jahn-Teller instability, Ni plays the key role in driving the instability and hence, a structural transformation. Thus, the concentration of Ni is a key factor in relative stabilities of structural phases in these compounds. Therefore, when Fe concentration, substituting Ni, exceeds a critical limit (here $x = 0.75$), the hybridization near the Fermi level, driven by Ni, weakens, diminishing the Jahn-Teller instability. This is the reason behind the stabilization of the austenite phase in Fe@Ni-Cu@Mn compounds shown in Fig. 2(a). The addition of Cu instead of Mn further weakens Ni-Mn hybridization stabilizing the austenite phases ($y = 0.25, 0.5$) more. The very similar features in the density of states near the Fermi level for Co@Ni-Cu@Mn compounds [Fig. 2(b)] offer the same

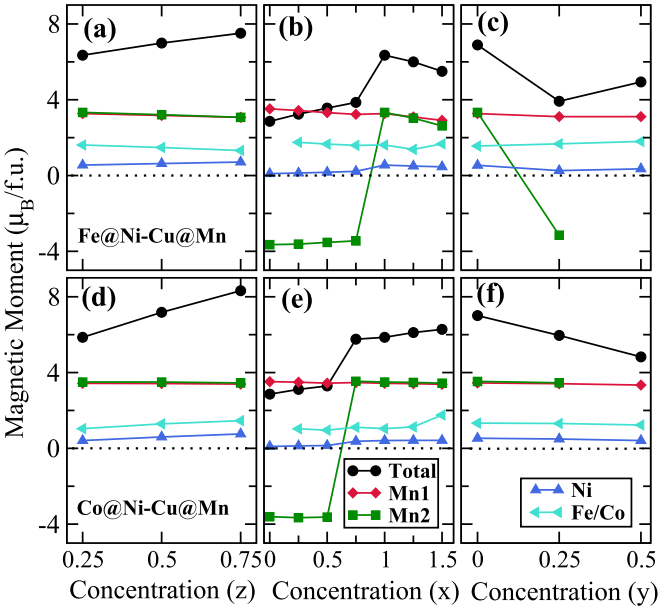

FIG. 3. Variations in the calculated total and atomic magnetic moments (in μ_B/f.u.) with z ($x = 1$, $y = 0$), x ($y = 0$, $z = 0.25$), and y ($x = 0.75$, $z = 0.5$) for [(a)–(c)] $Ni_{2-x}Fe_xMn_{1+z-y}Cu_ySb_{1-z}$ and [(d)–(f)] $Ni_{2-x}Co_xMn_{1+z-y}Cu_ySb_{1-z}$ systems in their austenite phases. Mn1 and Mn2 denote Mn atoms at its own site and at other sites in $L2_1$ structures, respectively.

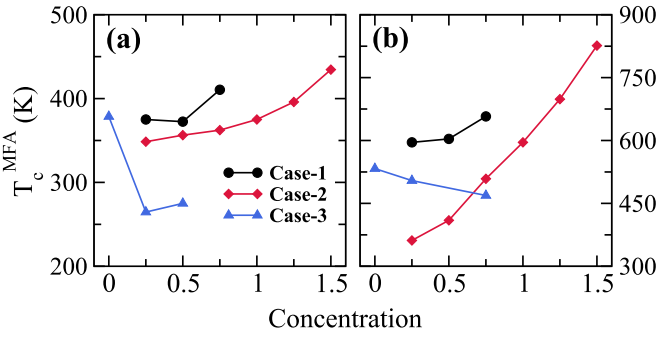

FIG. 4. Variations of the mean-field approximated Curie temperatures (T_c^{MFA}) with concentrations x, y, and z for (a) $Ni_{2-x}Fe_xMn_{1+z-y}Cu_ySb_{1-z}$ and (b) $Ni_{2-x}Co_xMn_{1+z-y}Cu_ySb_{1-z}$ systems in their austenite phases. Case 1 stands for variations with z ($x = 1$, $y = 0$). Case 2 shows variations with x ($y = 0$, $z = 0.25$). Case 3 is for variations with y ($x = 0.75$, $z = 0.5$).

explanation behind the origin of the stability of austenite phases for the compounds with given compositions.

2. *Understanding magnetic properties from effective exchange interactions*

In this subsection, we understand the fundamentals of the variations in magnetic moments and Curie temperatures by inspecting the magnetic exchange interactions. We find interesting trends in magnetic moments in some of the cases if we analyze the effects of substitutions with different elements systematically. For example, in $Ni_{2-x}Fe_xMn_{1+z-y}Cu_ySb_{1-z}$(Fe@Ni-Cu@Mn) family, a large magnetic moment is observed for high concentrations of Fe in systems with $y = 0$, $z = 0.25$. In Fig. 1, it can be seen that there is a slight increase in magnetic moment initially upon Fe substitution for compositions with $z = 0.25$, $y = 0$. In between the compositions with $x = 0.75$ and $x = 1$, a sudden jump in magnetic moment occurs; it decreases again linearly if more Fe is added to the system. However, the Curie temperature increases throughout the whole concentration range of Fe in this case. If z (Mn concentration) is further increased, the same behavior of magnetization and T_c^{MFA} are obtained with a less amount of Fe in the system. With a fixed Fe content, if Cu is added in this composition range, both magnetic moment and Curie temperature decrease in the system. To analyze the trends, we adopt the following procedure: We inspect the variations in the total and atomic moments by (a) first considering systems with no Cu ($y = 0$), a fixed amount of Fe/Co ($x = 1$), and excess Mn ($z \geqslant 0.25$); (b) then considering systems with no Cu ($y = 0$), a fixed concentration of excess Mn ($z = 0.25$), and amount of Fe/Co variable; and (c), finally, considering systems where Fe/Co concentration and an amount of excess Mn are fixed ($x = 0.75, z = 0.5$), the amount of Cu, y, being the only variable. The results are shown in Fig. 3. The variations in Curie temperatures are investigated by the same procedure and shown in Fig. 4. The effective interatomic exchange interactions $J_{\mathrm{eff}}^{\mu\nu} = \sum_j J_{0j}^{\mu\nu}$, 0 fixed on sublattice μ and j sites belong to sublattice ν ($J_{ij}^{\mu\nu}$, the magnetic exchange parameters for the atoms i, j belonging to μ, ν sublattices), shown in Fig. 5, are used to analyze the results.

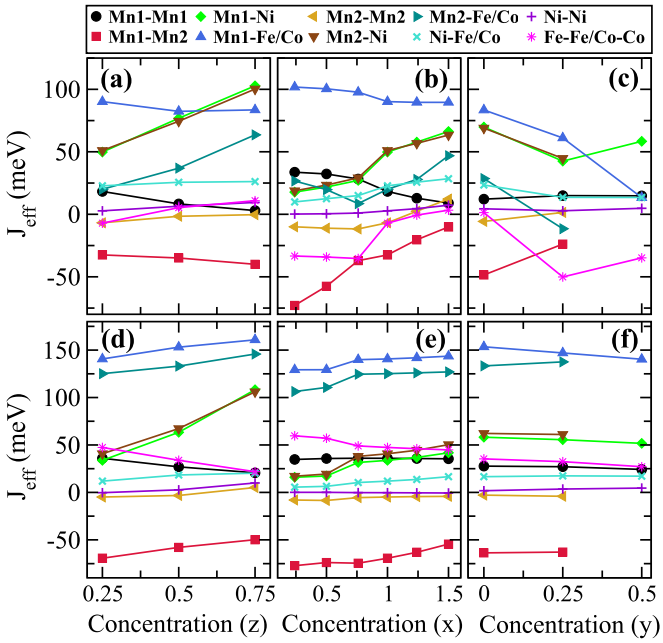

FIG. 5. Variations of the calculated effective exchange coupling constants with z ($x = 1$, $y = 0$), x ($y = 0$, $z = 0.25$) and y ($x = 0.75$, $z = 0.5$) for [(a)–(c)] $Ni_{2-x}Fe_xMn_{1+z-y}Cu_ySb_{1-z}$ and [(d)–(f)] $Ni_{2-x}Co_xMn_{1+z-y}Cu_ySb_{1-z}$ systems in their austenite phases. Mn1 and Mn2 denote Mn atoms at its own site and at other sites in $L2_1$ structure, respectively.

Figures 3(a) and 3(d) show that for a fixed and high content of substituted Fe/Co, the substitution of excess-Mn at the expense of Sb leads to increase of the total magnetic moment with Mn content. This is somewhat counterintuitive due to the following: stoichiometric Ni_2MnSb has a magnetic moment of nearly 4 μ_B/f.u. contributed primarily by Mn. Existing results show that the moment decreases gradually with excess Mn content as the Mn spins at different sites align antiparallel. An increasing trend of the moment is only seen when Fe substitutes Mn [28] or Co substitutes Ni [25–27]; the increases, however, were not as large as observed here. A look at the atomic moments reveals that Fe/Co being stronger magnets than Ni, along with the parallel alignment of Mn spins at different sites, are behind high magnetic moments of the system. In this case, the Curie temperature (T_c^{MFA}) also increases with z for both the systems, as can be seen in Fig. 4 (referred to as case 1). Insights into such qualitative behavior can be obtained from the variations of effective magnetic exchange interactions, shown in Figs. 5(a) and 5(d). We find that for both Fe- and Co-substituted systems, the dominant antiferromagnetic and ferromagnetic J_{eff} are due to the Mn1-Mn2 and Mn1(Mn2)-Ni pairs, respectively. The ferromagnetic component is strenghthened by the interactions between substituted Fe/Co and Mn. In case of Fe substituted system, the antiferromagnetic $J_{\mathrm{eff}}^{\mathrm{Mn1\text{-}Mn2}}$ increases slightly, although the dominant ferromagnetic J_{eff}s like $J_{\mathrm{eff}}^{\mathrm{Mn1(Mn2)\text{-}Ni}}$, $J_{\mathrm{eff}}^{\mathrm{Mn1\text{-}Fe}}$ increase significantly. The overall increase in ferromagnetic effective exchange interactions results into a growing trend in Curie temperature with z, the concentration of excess Mn [Fig. 5(a)]. In case of a Co-substituted system, along with the increased

ferromagnetic J_{eff}s, decreasing antiferromagnetic $J_{eff}^{Mn1\text{-}Mn2}$s as a function of z [Fig. 5(d)] explains the trend in Curie temperature of the system [Fig. 4(b), case 1]. The higher Curie temperatures in Co-substituted systems, in comparison with Fe-substituted ones, can be interpreted as due to quantitatively larger ferromagnetic interactions in the former.

Interesting jumps in magnetization are observed [Figs. 3(b) and 3(e)] at a critical concentration of Fe/Co in systems with no Cu and Mn content 25% in excess ($z = 0.25$, $y = 0$). The atomic moments reveal that such discontinuous jumps in magnetic moments are solely due to the change in orientation of the Mn spins: from an antiparallel to a parallel alignment. The continuous increase in Curie temperature, as shown in Fig. 4 (case 2), can be attributed to the significant increase in ferromagnetic J_{eff}s due to Mn1(Mn2)-Ni and Mn1(Mn2)-Fe pairs and the decrease in antiferromagnetic J_{eff} due to Mn pairs. One important difference between the two systems can be immediately noticed. While the T_c for the Co-substituted system rises sharply to a very high value, this is not so for the Fe-substituted system. The origin of this difference is in the significant presence of antiferromagnetic interactions in Fe-substituted compounds for low concentrations of Fe.

The variations in moments with content of Cu (y) when Mn and Fe content held fixed ($z = 0.5$, $x = 0.75$), are shown in Figs. 3(c) and 3(f). For the Fe@Ni-Cu@Mn system, the variation of the moment is nonmonotonic. With the addition of Cu, the moment first decreases due to the antiparallel alignment of Mn spins at different sites. With Cu content being 0.5 and beyond, there is no Mn at sites other than its original, for the spins to align antiparallel. The total moment, therefore, increases again. In the Co@Ni-Cu@Mn system, Cu addition does not affect the magnetic orientation of the Mn atoms leading to a monotonic variation of the total moment. The differences in the variations of the moments in these two cases are reflected in the variations of the Curie temperatures (Fig. 4, case 3). The calculated effective exchange parameters [Figs. 5(c) and 5(f)] show that the presence of substantial antiferromagnetic interactions at low concentrations of Cu and subsequent reductions in the dominant Mn-Co ferromagnetic interaction, due to reduced content of Mn in the Co@Ni-Cu@Mn system, leads to monotonic decrease of its T_c with Cu concentration. In the Fe@Ni-Cu@Mn system, the nonmonotonic behavior of T_c, with y, can similarly be interpreted.

This analysis by systematic variations of the contents of the substituents implies that the contents of the substituents for cosubstitution are critical to obtain the target properties, as they renormalize the magnetic exchange interactions significantly. The reason for a larger number of compounds satisfying the criteria laid out in Sec. III A in Co-substituted family is due to substantially larger ferromagnetic components in magnetic exchange interactions that pull the magnetic moments up. On the other hand, the addition of Cu in place of Mn reduces the possibilities of antiferromagnetic interactions bringing the moments down. At the same time, Cu addition reduces the strengths of the exchange interactions, pushing T_c closer to room temperature. The large and stable ferromagnetic exchange interactions in this family can also be correlated to the stable austenite phases in almost all select compounds in this family.

IV. CONCLUSIONS

In this work, we have established that cosubstitution by transition metals Fe, Co, and Cu in Mn-excess Sb-deficient Ni-Mn-Sb compounds can lead to significant changes in magnetic entropy, driven by a second-order magnetic transition near room temperature. Thus, cosubstitution in Ni-Mn-Z Heuslers compounds can emerge as an efficient way to obtain reversible MCE, exploiting the advantages of second-order phase transitions over those in a first-order magnetostructural transition. We find that the cosubstitution provides a wider scope of tuning the physical parameters like magnetic moments and magnetic transition temperature as well as of stabilization of the Heusler phase down to very low temperatures. The calculated changes in the magnetic entropy, for most of the materials, are comparable to those obtained in off-stoichiometric Heusler compounds undergoing the first-order transition. This paper thus offers a broader scope of synthesis and exploration of large MCE near room temperature by cosubstitution in other compounds of the Heusler family.

ACKNOWLEDGMENTS

The authors gratefully acknowledge the Department of Science and Technology, India for the computational facilities under Grant No. SR/FST/P-II/020/2009 and IIT Guwahati for the PARAM supercomputing facility.

[1] I. Hughes, M. Däne, A. Ernst, W. Hergert, M. Lüders, J. Poulter, J. Staunton, A. Svane, Z. Szotek, and W. Temmerman, Nature **446**, 650 (2007).
[2] G. Brown, J. Appl. Phys. **47**, 3673 (1976).
[3] M. Kuz'Min and A. Tishin, Cryogenics **33**, 868 (1993).
[4] A. Morozkin, R. Nirmala, and S. Malik, J. Magn. Magn. Mater. **378**, 221 (2015).
[5] V. K. Pecharsky and K. A. Gschneidner Jr, Phys. Rev. Lett. **78**, 4494 (1997).
[6] M. Pasquale, C. P. Sasso, L. H. Lewis, L. Giudici, T. Lograsso, and D. Schlagel, Phys. Rev. B **72**, 094435 (2005).
[7] A. K. Pathak, M. Khan, I. Dubenko, S. Stadler, and N. Ali, Appl. Phys. Lett. **90**, 262504 (2007).
[8] T. Krenke, E. Duman, M. Acet, E. F. Wassermann, X. Moya, L. Mañosa, and A. Planes, Nat. Mater. **4**, 450 (2005).
[9] S. E. Muthu, N. R. Rao, M. M. Raja, D. R. Kumar, D. M. Radheep, and S. Arumugam, J. Phys. D: Appl. Phys. **43**, 425002 (2010).
[10] M. Khan, N. Ali, and S. Stadler, J. Appl. Phys. **101**, 053919 (2007).
[11] S. Singh, L. Caron, S. W. D'Souza, T. Fichtner, G. Porcari, S. Fabbrici, C. Shekhar, S. Chadov, M. Solzi, and C. Felser, Adv. Mater. **28**, 3321 (2016).
[12] S. Ghosh, A. Ghosh, and K. Mandal, J. Alloys. Compd. **746**, 200 (2018).

[13] G. Cavazzini, F. Cugini, M. Gruner, C. Bennati, L. Righi, S. Fabbrici, F. Albertini, and M. Solzi, Scr. Mater. **170**, 48 (2019).

[14] B. Gao, J. Shen, F. Hu, J. Wang, J. Sun, and B. Shen, Appl. Phys. A **97**, 443 (2009).

[15] J.-M. Lee, Y.-M. Oh, K. Euh, and S.-B. Kang, Met. Mater. Int. **15**, 459 (2009).

[16] R. Kainuma, Y. Imano, W. Ito, H. Morito, Y. Sutou, K. Oikawa, A. Fujita, K. Ishida, S. Okamoto, O. Kitakami *et al.*, Appl. Phys. Lett. **88**, 192513 (2006).

[17] M. Khan, I. Dubenko, S. Stadler, and N. Ali, J. Appl. Phys. **97**, 10M304 (2005).

[18] D. Soto-Parra, X. Moya, L. Mañosa, A. Planes, H. Flores-Zuñiga, F. Alvarado-Hernandez, R. Ochoa-Gamboa, J. A. Matutes-Aquino, and D. Rios-Jara, Philos. Mag. **90**, 2771 (2010).

[19] A. K. Pathak, I. Dubenko, C. Pueblo, S. Stadler, and N. Ali, J. Appl. Phys. **107**, 09A907 (2010).

[20] A. Gomes, M. Khan, S. Stadler, N. Ali, I. Dubenko, A. Takeuchi, and A. Guimarães, J. Appl. Phys. **99**, 08Q106 (2006).

[21] S. Stadler, M. Khan, J. Mitchell, N. Ali, A. M. Gomes, I. Dubenko, A. Y. Takeuchi, and A. P. Guimarães, Appl. Phys. Lett. **88**, 192511 (2006).

[22] D. Soto, F. A. Hernández, H. Flores-Zúñiga, X. Moya, L. Manosa, A. Planes, S. Aksoy, M. Acet, and T. Krenke, Phys. Rev. B **77**, 184103 (2008).

[23] T. Krenke, E. Duman, M. Acet, X. Moya, L. Mañosa, and A. Planes, J. Appl. Phys. **102**, 033903 (2007).

[24] S. Ghosh and S. Ghosh, Phys. Rev. B **101**, 024109 (2020).

[25] Z. Han, D. Wang, C. Zhang, H. Xuan, J. Zhang, B. Gu, and Y. Du, J. Appl. Phys. **104**, 053906 (2008).

[26] A. K. Nayak, K. Suresh, and A. Nigam, J. Phys. D: Appl. Phys. **42**, 035009 (2009).

[27] A. K. Nayak, K. Suresh, and A. Nigam, J. Phys. D: Appl. Phys. **42**, 115004 (2009).

[28] R. Sahoo, A. K. Nayak, K. Suresh, and A. Nigam, J. Appl. Phys. **109**, 123904 (2011).

[29] M. Zelený, A. Sozinov, L. Straka, T. Björkman, and R. M. Nieminen, Phys. Rev. B **89**, 184103 (2014).

[30] V. V. Sokolovskiy, P. Entel, V. D. Buchelnikov, and M. E. Gruner, Phys. Rev. B **91**, 220409(R) (2015).

[31] A. Perez-Checa, J. Feuchtwanger, J. Barandiaran, A. Sozinov, K. Ullakko, and V. Chernenko, Scr. Mater. **154**, 131 (2018).

[32] P. E. Blöchl, Phys. Rev. B **50**, 17953 (1994).

[33] G. Kresse and D. Joubert, Phys. Rev. B **59**, 1758 (1999).

[34] G. Kresse and J. Furthmüller, Phys. Rev. B **54**, 11169 (1996).

[35] J. P. Perdew, K. Burke, and M. Ernzerhof, Phys. Rev. Lett. **77**, 3865 (1996).

[36] H. Ebert, D. Koedderitzsch, and J. Minar, Rep. Prog. Phys. **74**, 096501 (2011).

[37] A. I. Liechtenstein, M. Katsnelson, V. Antropov, and V. Gubanov, J. Magn. Magn. Mater. **67**, 65 (1987).

[38] V. V. Sokolovskiy, V. D. Buchelnikov, M. A. Zagrebin, P. Entel, S. Sahoo, and M. Ogura, Phys. Rev. B **86**, 134418 (2012).

[39] M. Meinert, J.-M. Schmalhorst, and G. Reiss, J. Phys.: Condens. Matter **23**, 036001 (2010).

[40] D. P. Landau and K. Binder, *A Guide to Monte Carlo Simulations in Statistical Physics* (Cambridge University Press, New York, 2014).

[41] M. Zagrebin, V. Sokolovskiy, and V. Buchelnikov, J. Phys. D: Appl. Phys. **49**, 355004 (2016).

[42] A. Kundu, S. Ghosh, and S. Ghosh, Phys. Rev. B **96**, 174107 (2017).

[43] See Supplemental Material at http://link.aps.org/supplemental/10.1103/PhysRevMaterials.4.025401 for detailed discussions on computational methods to calculate Curie temperature in the austenite phase, the maximum change in magnetic entropy associated with the second-order magnetic transition, the results of total energy calculations with distortion for some selected compositions, and their total and atom-projected density of states.

[44] P. Meyer, M. Phil thesis, School of Mathematics and Computing, University of Derby (2000).

[45] N. Singh, E. Dogan, I. Karaman, and R. Arróyave, Phys. Rev. B **84**, 184201 (2011).

[46] V. D. Buchelnikov, V. V. Sokolovskiy, H. C. Herper, H. Ebert, M. E. Gruner, S. V. Taskaev, V. V. Khovaylo, A. Hucht, A. Dannenberg, M. Ogura, H. Akai, M. Acet, and P. Entel, Phys. Rev. B **81**, 094411 (2010).

[47] S. Ghosh and S. Ghosh, Phys. Rev. B **99**, 064112 (2019).

[48] A. Ghosh and K. Mandal, Appl. Phys. Lett. **104**, 031905 (2014).

[49] V. Sánchez-Alarcos, V. Recarte, J. Pérez-Landazábal, and G. Cuello, Acta Mater. **55**, 3883 (2007).

[50] C.-M. Li, H.-B. Luo, Q.-M. Hu, R. Yang, B. Johansson, and L. Vitos, Phys. Rev. B **84**, 024206 (2011).

[51] A. Chakrabarti, M. Siewert, T. Roy, K. Mondal, A. Banerjee, M. E. Gruner, and P. Entel, Phys. Rev. B **88**, 174116 (2013).

[52] M. Meinert, J.-M. Schmalhorst, and G. Reiss, J. Phys.: Condens. Matter **23**, 116005 (2011).